Investigation of octupole deformed fragments decaying from even-even isotopes of $^{222–230}$Th*

Shivani Jain [1,*] Raj Kumar [1] S. K. Patra,[2,3] and Manoj K. Sharma[1]

[1]*School of Physics and Materials Science, Thapar Institute of Engineering & Technology, Patiala 147004, Punjab, India*
[2]*Institute of Physics, Bhubaneswar 751005, India*
[3]*Homi Bhabha National Institute, Training School Complex, Anushakti Nagar, Mumbai 400094, India*

(Received 7 November 2021; accepted 17 February 2022; published 7 March 2022)

Background: In earlier studies, spherical and quadrupole deformed nuclei with closed shells were found to be the most probable fission fragments in the decay of heavy-mass compound nuclei at low excitation energies. Recently, the disintegration of heavy-mass actinides gave evidence of pear-shaped fission fragments, in the mass-asymmetric region, due to extra stability provided by the shell-stabilized octupole deformed ^{144}Ba ($Z = 56$) nucleus.
Purpose: In our theoretical work, we have done an exercise to analyze the possibility of octupole deformed fragments in the decay of light- and heavy-mass isotopes of thorium, i.e., ^{222,224,226,228,230}Th*.
Method: To carry forward the above idea, the mass and charge dispersions of chosen Th isotopes have been analyzed by including deformations (up to β_3) and related cold optimum orientations within the dynamical cluster-decay model (DCM), which is based on the collective clusterization approach of quantum mechanical fragmentation theory. The above analysis is worked out at low excitation energy, which corresponds to the cold synthesis criteria.
Results: In the decay of considered Th isotopes, the minima of fragmentation potential and peaks of preformation probability appear in two regions, near symmetric and asymmetric, respectively due to the presence of quadrupole (β_2) and octupole deformations (β_3) of decay fragments. However, the emission of β_3-deformed fission fragments is prominent in the heavier isotopes of Th, i.e., ^{226,228,230}Th*. The above result is in agreement with the experimentally obtained mass and charge distributions.
Conclusions: The disintegration of thorium isotopes into octupole deformed fragments in the asymmetric region signifies their relative stability, which is enhanced for ^{144}Ba ($Z = 56$) or in its vicinity.

DOI: 10.1103/PhysRevC.105.034605

I. INTRODUCTION

Comprehensive knowledge is required to understand the complex behavior of the nuclear fragments emitted in a variety of decay channels. Such decaying fragments behave as a source of production of new isotopes/elements away from the beta-stability line, which in turn help to extend the nuclear periodic table. The newly discovered nuclei are further harvested for fundamental understanding related to various nuclear properties and the associated applications in diverse areas such as radiation, astro sciences, medical and health sectors, etc.

In general, the possible target-projectile combination forms an excited compound nucleus (CN), and subsequently disintegrates into binary fragments under various conditions, such as excitation energy/temperature, angular momentum, deformations, orientations, etc. With the effect of these factors, the deexcitation of the CN may lead to different decay mechanisms, viz., evaporation residues (ERs) or equivalently light-mass fragments (LFs), intermediate-mass fragments (IMFs), heavy-mass fragment (HMFs), and fission processes. The dominance of these decay modes varies with the mass and excitation energy of CN. In the present work, we will focus on the study of the fission process, which is dominant in the heavy-mass region.

The deexcitation of a compound nucleus, formed via ^{208}Pb-based (cold fusion process) or ^{48}Ca-induced reactions (hot fusion process), respectively, at low ($E^*_{CN} \approx$ 10–20 MeV) [1,2] and high excitation energies ($E^*_{CN} \approx$ 35–45 MeV) [3,4] may lead to the production of new elements. The low and high ranges of E^*_{CN} correspond to the incident energy $E_{\mathrm{c.m.}}$, which may spread across the Coulomb barrier [5,6]. In the work of Gupta and his collaborators [7], the fragmentation of an excited CN was discussed by considering quadrupole deformations along with the cold and hot optimum orientation effects. Here, the cold optimum case corresponds to the largest interaction distance between the decaying nuclear partners, which in turn gives the lowest barrier height. On the other hand, the smallest interaction distance and highest barrier height illustrates the hot optimum case. On the basis of these criteria, the elongated (or cold) and compact (or hot) configurations of deformed nuclear partners are employed to study the fusion-fission process, respectively, at low and high excitation energies; see Refs. [8–11]. Also, it has been investigated that, like spherical nuclei, quadrupole deformed nuclei of closed shells are the most probable decaying fragments from compound nuclei in the heavy-mass region [12–22].

*jain.shivani04@gmail.com

Similarly to quadrupole (β_2) deformed nuclei, the study of pear-shape octupole (β_3) deformed nuclei is important in order to extract the appropriate nuclear structure [23,24]. In our recent work [25], we determined that the octupole deformed nuclei of pear shapes, which break symmetry along the reflection axis, modiy the value of θ_{opt}, compared to the values obtained for the β_2-deformed case. In a recent work [26], it was realized that this new set of optimum orientations related to the elongated (or cold) configuration of octupole deformed nuclei shows relatively larger impact on the fusion/Coulomb barrier, as compared to the compact (or hot) configuration case. In view of this, it would be interesting to analyze the possibility of elongated octupole deformed fission fragments emitting from a compound nucleus which is formed at low excitation energy.

In the recent experimental work [27], the fission dynamics of heavy-mass actinides (e.g., ^{230}Th, ^{234,236}U, ^{240}Pu, ^{246}Cm, ^{250}Cf, and ^{258}Fm) was discussed, and the authors confirmed unambiguously the emission of octupole deformed nuclei/fragments of atomic number 56, i.e., ^{144}Ba, in the asymmetric region at low excitation energy. Such analysis has motivated us to study the application of cold optimum orientations of octupole deformed fragments in the fission dynamics of even-even isotopes of Th, i.e., $^{222-230}$Th*. This analysis is exercised at a low value of E^*_{CN}, which corresponds to the cold synthesis of elements. To carry forward with this idea, we are using the dynamical cluster-decay model (DCM) [28–30], which is applied to probe various decay mechanisms of CN formed in heavy-ion induced reactions. The model has been built on the collective clusterization approach of quantum mechanical fragmentation theory (QMFT) [31–33].

In the present work, to have an explicit understanding of higher-order deformation (up to β_3) and related cold optimum orientations, the fission of Th isotopes is discussed by a comparative analysis of fission fragment distributions using mass asymmetry (η_A) and charge asymmetry (η_Z) parameters. In the above analysis, the minima of the potential observed in the fission region helps in determining the peak value of preformation probability for the fission fragments. On the basis of this, the identification of the most probable fission fragments in reference to η_A and η_Z coordinates is also done. Note that the neck-length parameter optimized for the ^{224}Th* nucleus in reference to the available experimental data for below-barrier energies [34] has been worked out for the fragmentation analysis of the remaining isotopes of Th. In DCM, the neck-length parameter $\triangle R$, the only parameter, is utilized to fix the first turning point, where the preformed fragments start to penetrate through the interaction potential. Relevant to the study undertaken, Sec. II describes the collective clusterization approach of DCM. In Sec. III, a detailed discussion is given on the results obtained by incorporating the deformations up to β_3 with cold optimum orientation effects. Finally, a brief summary is given in Sec. IV.

II. METHODOLOGY

A. The dynamical cluster-decay model (DCM)

In the present work, the decay of excited compound nuclei (CN) has been studied using the collective clusterization approach of the dynamical cluster-decay model (DCM) [28–30]. The model is derived using collective coordinates of mass and charge asymmetry parameters $\eta_A = \frac{|A_1-A_2|}{A_1+A_2}$ and $\eta_Z = \frac{|Z_1-Z_2|}{Z_1+Z_2}$ (here 1 and 2 correspond to the decaying binary fragments), relative separation distance R, nuclear deformations $\beta_{\lambda i}$ ($\lambda = 2, 3$; $i = 1, 2$), orientation (θ_i), etc. Depending on these coordinates, the fission cross section of decaying fragments is given as

$$\sigma_{fis}(A_1, A_2) = \frac{\pi}{k^2}\sum_{\ell=0}^{\ell_{\max}}(2\ell+1)P_0P. \tag{1}$$

Here, the fission fragments decaying from considered Th isotopes into the mass/charge-symmetric and -asymmetric regions have mass and charge number ranges of $A_2 = \frac{A_{CN}}{2} \pm 35$ and $Z_2 = \frac{Z_{CN}}{2} \pm 15$, respectively. Note that A_{CN} and Z_{CN} are the mass and charge numbers of the compound nucleus, respectively. $k = \sqrt{\frac{2\mu E_{\text{c.m.}}}{\hbar^2}}$, and $\mu = m[A_1A_2/(A_1 + A_2)]$ is the reduced mass. m is the nucleon mass. In the above expression, the term P_0 is the preformation probability, which contains structural information of the compound nuclear system. Based on the QMFT, the P_0 is calculated by solving the stationary Schrodinger equation in η coordinates [35],

$$\left\{-\frac{\hbar^2}{2\sqrt{B_{\eta\eta}}}\frac{\partial}{\partial\eta}\frac{1}{\sqrt{B_{\eta\eta}}}\frac{\partial}{\partial\eta} + V_R(\eta, T)\right\}\psi^\nu(\eta) = E^\nu\psi^\nu(\eta), \tag{2}$$

where $\nu = 0$ refers to the ground state and $\nu = 1, 2, 3, \dots$ correspond to the excited states. Note that, in the above equation, η can be mass (η_A) or charge (η_Z) dependent, and consequently the solution of Eq. (2) gives P_0 as a function of mass-asymmetry parameter η_A [32],

$$P_0(\eta_A) = |\psi(\eta(A_i))|^2\sqrt{B_{\eta_A\eta_A}}\frac{2}{A_{CN}}. \tag{3}$$

On the other hand, the preformation probability as a function of charge-asymmetry parameter η_Z reads as [36]

$$P_0(\eta_Z) = |\psi(\eta(Z_i))|^2\sqrt{B_{\eta_Z\eta_Z}}\frac{2}{Z_{CN}}. \tag{4}$$

In Eqs. (3) and (4), the states $\psi(\eta(A_i))$ and $\psi(\eta(Z_i))$, respectively, are the vibrational states. For fission from excited states, the possible outcomes related to the excitations of higher vibrational states are considered by assuming them to be Boltzmann-like wave functions, such as

$$|\psi|^2 = \sum_{\nu=0}^{\infty}|\psi^\nu|^2\exp(E^\nu/T). \tag{5}$$

In the above equations, $B_{\eta_A\eta_A}$ and $B_{\eta_Z\eta_Z}$ are smooth hydrodynamical parameters; for more details see [37]. In Eq. (1), the other term P is called the penetration probability. This means the preformed cluster/fragment formed inside the potential pocket starts penetrating through the first classical turning point, i.e., $R = R_a = R_1(\alpha_1, T) + R_2(\alpha_2, T) + \triangle R$, and terminates through the second turning point R_b, such that $V(R_a) = V(R_b)$; for clarity see Fig. 1, where total interaction potential is plotted as a function of separation distance. The idea of introducing neck-length parameter $\triangle R$ within the

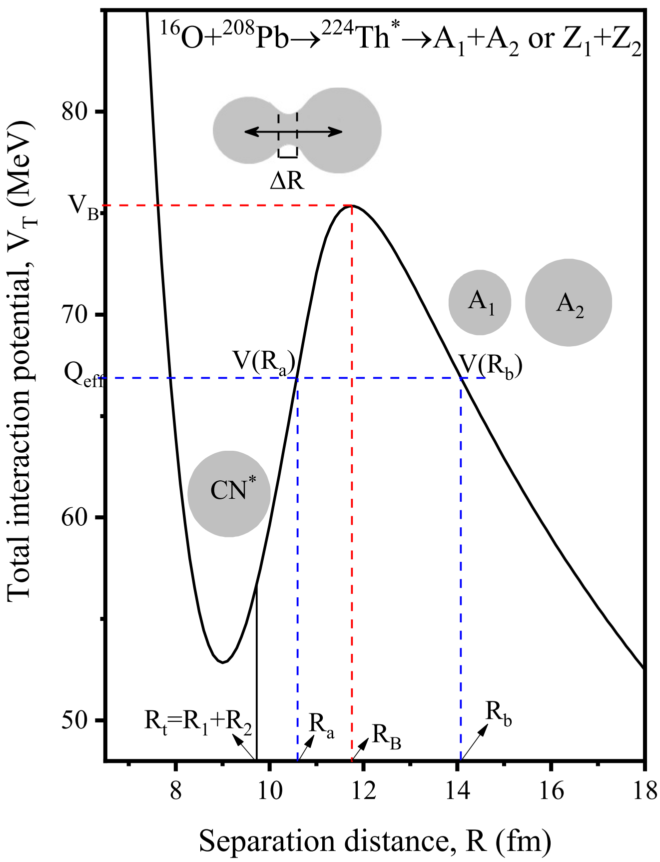

FIG. 1. The variation of total interaction potential V_T (MeV) as a function of separation distance R (fm) between the colliding nuclear partners is shown for the $^{16}O + ^{208}Pb \rightarrow ^{224}Th^*$ reaction. Here, $R_a = R_1(\alpha_1, T) + R_2(\alpha_2, T) + \triangle R$ defines the first turning point.

DCM [38–40] is similar to the saddle- [41,42] and scission-point [43] statistical fission models. The permissible value of $\triangle R$ lies in the nuclear proximity range of about 2 fm, since the surface interaction between two fragments can take place around this range of $\triangle R$ to experience the nuclear force.

The term P in Eq. (1) is calculated using the Wentzel-Kramers-Brillouin (WKB) approximation and is given as [44]

$$P = \exp\left[-\frac{2}{\hbar}\int_{R_a}^{R_b}\{2\mu[V(R) - Q_{\text{eff}}]\}^{1/2} dR\right]. \quad (6)$$

In the above equation, Q_{eff} is the effective Q value of the decay channel.

In solving the Schrodinger equation, Eq. (2), a term $V_R(\eta, T)$, defined as the fragmentation potential, is given as

$$V_R(\eta, T) = \sum_{i=1}^{2}[V_{LDM}(A_i, Z_i, T)] + \sum_{i=1}^{2}[\delta U_i]\exp\left(-T^2/T_0^2\right) + V_C(R, Z_i, \beta_{\lambda i}, \theta_i, T) + V_\ell(R, A_i, \beta_{\lambda i}, \theta_i, T) + V_N(R, A_i, \beta_{\lambda i}, \theta_i, T). \quad (7)$$

Here, V_{LDM} is the temperature-dependent binding energy given by Davidson *et al.* [45], based on the semi-empirical mass formula of Seeger [46], for relevant details see Ref. [47]. The second term, i.e., shell corrections, is given by Myer and Switecki [48] with its T dependence from Davidson *et al.* [45]. The constituents of the total potential, i.e., the Coulomb potential (V_C), centrifugal potential (V_ℓ), and nuclear proximity potential (V_N), are functions of relative separation distance R, charge Z_i (mass A_i) number, temperature T, deformations $\beta_{\lambda i}$, and orientation θ_i degrees of freedom.

For spherical-deformed or deformed-deformed combinations, the repulsive Coulomb potential for coplanar oriented nuclei is given by [49]

$$V_C(R, Z_i, \beta_{\lambda i}, \theta_i, T) = \frac{Z_1Z_2e^2}{R} + 3Z_1Z_2e^2\sum_{i=1,2}\sum_{\lambda=2,3}\frac{1}{2\lambda+1}\frac{R_i^\lambda(\alpha_i, T)}{R(T)^{\lambda+1}} \times Y_\lambda^{(0)}(\theta_i)\left[\beta_{\lambda i} + \frac{4}{7}\beta_{\lambda i}^2 Y_\lambda^{(0)}(\theta_i)\right], \quad (8)$$

where $Y_\lambda^{(0)}(\theta_i)$ and $R_i(\alpha_i, T)$ represent the spherical harmonic functions and nuclear radius term, respectively. $\lambda = 2, 3$ stands for quadrupole and octupole deformations, respectively. The deformations of nuclei belonging to different mass regions are taken from the data table of Möller *et al.* [50]. The multipole expansion of the nuclear radius $R_i(\alpha_i, T)$ of deformed nuclei is described in terms of the spherical harmonic function [51,52], as given by

$$R_i(\alpha_i, T) = R_{0i}(T)\left[1 + \sum_{\lambda=2,3}\beta_{\lambda i}Y_\lambda^{(0)}(\alpha_i)\right]. \quad (9)$$

In the above expression, the T-dependent nuclear radius term $R_{0i}(T)$ is given as [53]

$$R_{0i}(T) = R_{0i}[1 + 0.0005T^2]. \quad (10)$$

Here, $R_{0i}(=1.28A_i^{1/3} - 0.76 + 0.8A_i^{-1/3})$ in fm [54] represents the radius of the equivalent spherical nucleus.

The temperature T is related to the excitation energy E^*_{CN} of the compound nucleus and given as [55]

$$E^*_{CN} = E_{\text{c.m.}} + Q_{in} = \frac{A_{CN}}{9}T^2 - T. \quad (11)$$

The rotational energy is given as [49]

$$V_\ell(R, A_i, \beta_{\lambda i}, \theta_i, T) = \frac{\hbar^2\ell(\ell+1)}{2I(T)}. \quad (12)$$

The nuclear proximity potential (V_N) is obtained from Blocki *et al.* [54]. Here, a collective formulation for deformed and coplanar oriented nuclei is considered [56–59], and V_N reads as

$$V_N(A_i, \beta_{\lambda i}, \theta_i, T) = 4\pi\bar{R}(T)\gamma b(T)\phi(s_0). \quad (13)$$

Note that V_N is a product of two terms: one, $[4\pi\bar{R}(T)\gamma b(T)]$, depends on the shape and geometry (relative orientation) of colliding nuclei; another term $[\phi(s_0)]$ is a function of single parameter, that is the minimum separation distance (s_0) between two colliding surfaces.

III. RESULTS AND DISCUSSION

In the present work, the main purpose is to analyze the influence of the elongated (or cold) configuration of octupole (β_3) deformed nuclei in the fission dynamics of even-even isotopes of thorium, i.e., $^{222-230}$Th*. The calculations are done at the low value of excitation energy E^*_{CN}, which is relevant for the cold synthesis process. To carry forward this idea, the deformations (up to β_3) and corresponding cold optimum orientation [25] are included in the framework of the dynamical cluster-decay model (DCM), which is developed on the basis of quantum mechanical fragmentation theory (QMFT). In the notion of QMFT, the probable decaying fragments/clusters are preborn inside the excited compound nucleus (CN) and then they penetrate through the interaction potential. With the use of the neck-length parameter $\triangle R$, which is the only parameter of DCM, one can fix the turning point of the barrier penetration.

To obtain knowledge of the turning points for preborn fragments of Th* isotopes, the neck-length parameter has to be optimized first, in view of the fission data at low excitation energies, corresponding to below-barrier energies. In view of this, Sec. III A explores the fission cross sections by including deformations (up to β_3) and cold optimum orientation effects in DCM for the ^{224}Th* compound nucleus and compares the results with available experimental data [34].[1] Further, in Sec. III B, the decay analysis of ^{222,224,226,228,230}Th* nuclei is illustrated at the same neck length $\triangle R$, obtained in fitting the data for the ^{16}O + ^{208}Pb reaction forming the ^{224}Th* compound nucleus. The above analysis is discussed in terms of the fragmentation potential [$V(\eta)$], which is minimized in reference to the mass (A_2) and charge (Z_2) numbers of the decaying fragment. Subsequently, the preformation probability P_0 [showing the inverse trend of $V(\eta)$] as a function of mass- (η_A) and charge-asymmetry (η_Z) coordinates illustrates, respectively, the mass- and charge-dispersion cases.

A. Fission cross sections for ^{224}Th* nucleus formed in ^{208}Pb based reaction

The minimization of fragmentation potential can be done in reference to the mass number A_2 as well as charge number Z_2 of the decaying nuclear partner from $^{224}_{90}$Th* and can be understood from Figs. 2 and 3, respectively. In Fig. 2, the mass number A_2 of the fragment and its isobars of different charge number Z_2 are shown along the horizontal and vertical axes, respectively. The color map represents the strength of fragmentation potential $V(\eta)$ for each A_2 and corresponding Z_2. The black spheres in the dark purple region show the lowest or minimum value of $V(\eta)$ for the decay fragments, which helps in choosing Z_2 for corresponding A_2 values. In other words, it is called the minimization of fragmentation potential in reference to the mass number of the CN. Further, in Fig. 3, for each Z_2 of decay fragment, there are isotopes

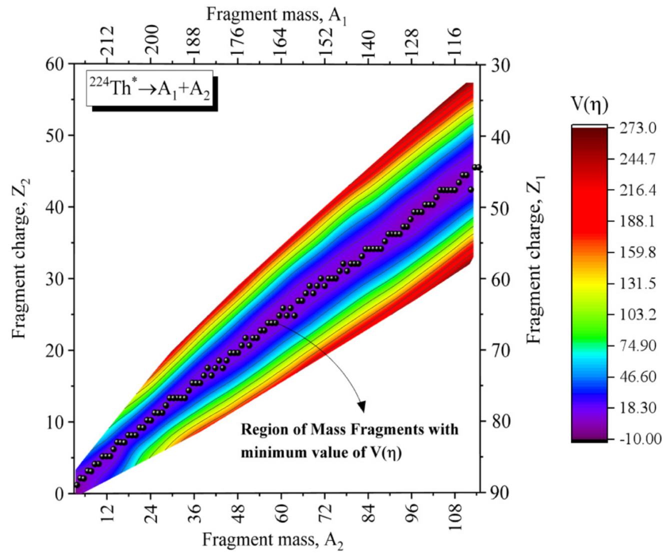

FIG. 2. The color map representing the fragmentation potential $V(\eta)$ for ^{224}Th* with respect to the fragment mass number A_2 having isobars (of different charge number Z_2). The mass A_1 and charge number Z_1 of the decaying partner are also shown in the top and right axes, respectively.

of different mass number A_2 and the spherical dots present in the dark blue color indicate the minima of $V(\eta)$ for an isotope. This way, one can find the minimization of $V(\eta)$ in reference to the charge number. Note that the mass and charge numbers of other decay partner are $A_1 = A - A_2$ and $Z_1 = Z - Z_2$, respectively, as shown in the opposite axes of A_2 and Z_2 of Figs. 2 and 3.

Further, the minimized potential $V(\eta)$ obtained for the disintegration of ^{224}Th* over the fragment mass range A_1 = 1–223 (and A_2 = 223–1) and charge number range Z_1 = 0–90

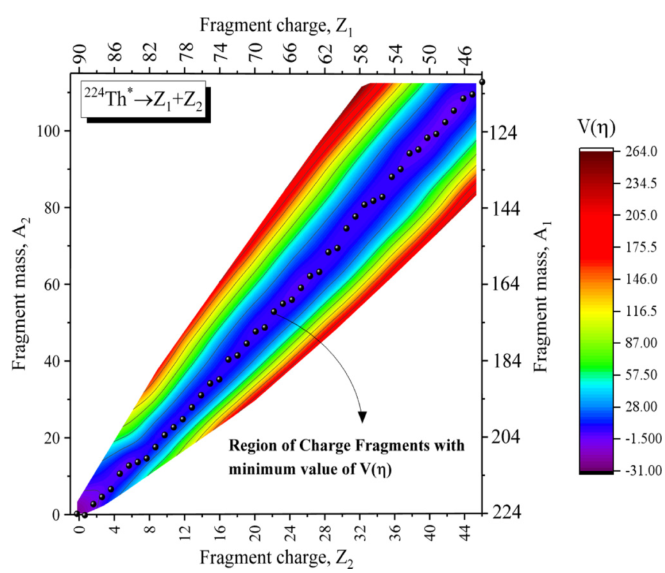

FIG. 3. The color map representing the fragmentation potential for ^{224}Th* with respect to the fragment charge number Z_2 having isotopes (of different mass number A_2).

[1]Note that, for the below-barrier region, the experimental measurements of fission cross sections are available only for the ^{16}O + ^{208}Pb → ^{224}Th* reaction.

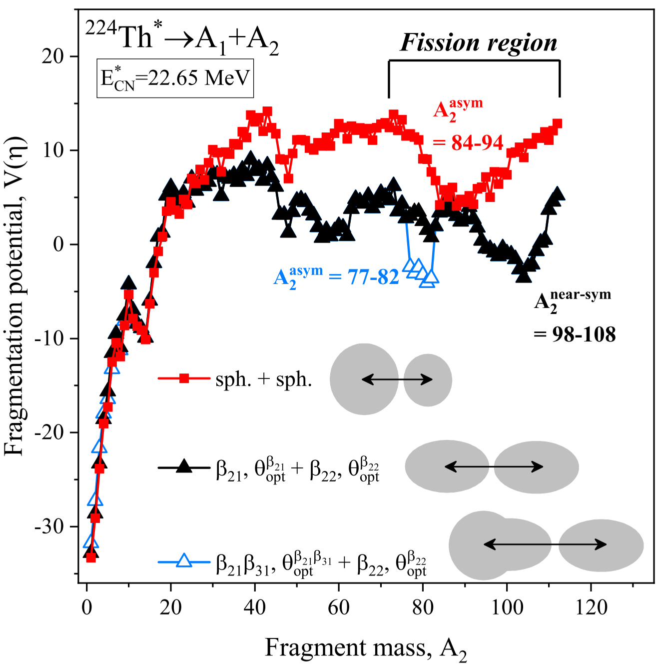

FIG. 4. The variation of minimized fragmentation potential with respect to the mass number of a decaying fragment, first for the spherical (sph.) case and then by including quadrupole (β_{2i}) and octupole (β_{3i}) deformations along with the related cold optimum orientations ($\theta_{\rm opt}^{\beta_{\lambda=2,3}}$). Here, $i = 1, 2$ refer to binary fragments A_1 and A_2, respectively.

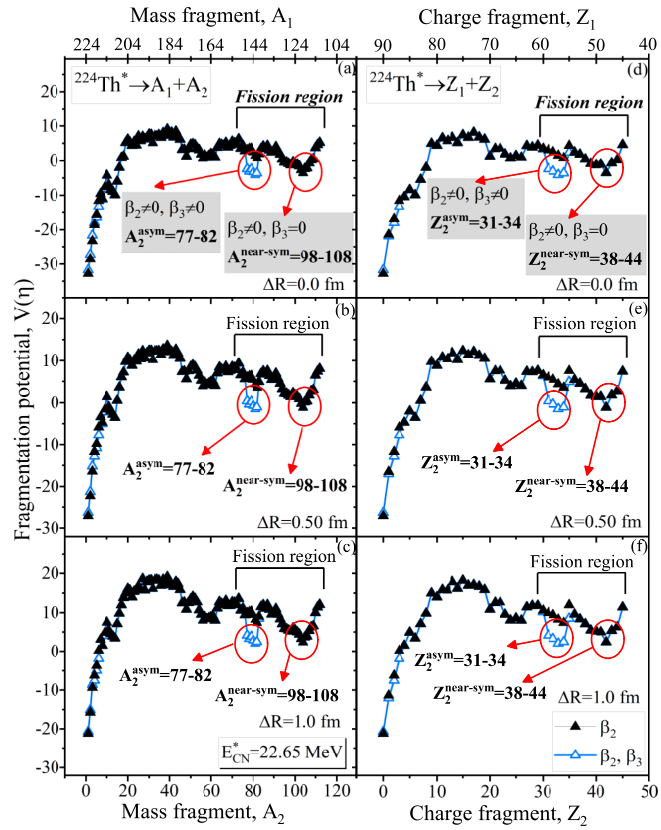

FIG. 5. The minimized fragmentation potential in reference to the fragment (a)–(c) mass A_2 and (d)–(f) charge number Z_2 of ^{224}Th*, at low excitation energy $E^*_{CN} = 22.65$ MeV and $\ell = 0\hbar$. The analysis is carried out at different values of neck-length parameter, i.e., $\triangle R = 0.0$, 0.5, and 1.0 fm.

(and $Z_2 = 90$–0) is discussed to understand the fragmentation structure with the inclusion of deformations (up to β_3) and cold optimum orientation effects. For an illustration, in Fig. 4, the role of quadrupole/octupole deformations and associated cold optimum orientation can be analyzed in reference to the spherical configuration of decaying fragments in the fission valley/region (marked in the figure). This region has the mass range of fission fragment A_2 from 72 to 112. It is clearly seen from this figure that, as one goes from spherical (sph.)+sph. to quadrupole (quad.)+quad. and then to quad.+octupole deformed pairs of decay fragments, the interaction distance increases, which in turn lowers the potential barrier with a larger extent. As a consequence, one can see that the minimization and structure of the fragmentation potential is modified, with a significant effect due to incorporation of deformation and orientation degrees of freedom.

In the comparative analysis of mass- and charge-dispersion cases, the behavior of $V(\eta)$ was tested for different values of neck-length parameters $\triangle R$ ($= 0.0$, 0.5, and 1.0 fm), as shown in Fig. 5. The above analysis is exercised at the lowest value of excitation energy, i.e., $E^*_{CN} = 22.35$ MeV, which is from the available experimental data of fission cross sections for the ^{16}O + ^{208}Pb → ^{224}Th* reaction at energies 22.65–25.29 MeV [34]. Since the present work is constrained to study the fission process of the above mentioned reaction, the relevant dips are specified in Fig. 5 for the fragmentation potential. One can clearly see the dip of $V(\eta)$ near the symmetric region ($\approx \frac{A_{CN}}{2} = 112$ and $\frac{Z_{CN}}{2} = 45$) for quadrupole (β_2) deformed nuclei associated with the cold optimum orientation. Afterwards, the presence of octupole (β_2, β_3) deformed fragments along with the optimum orientation defining their elongated configuration shows the minimum of $V(\eta)$ in the asymmetric region, which competes with that of the near-symmetric region. Also, it is important to note that the magnitude and structure of the potential observed in both the mass and charge distributions of ^{224}Th* are almost similar. The above results obtained due to β_2, β_3 deformations and related cold optimum orientations are consistently true for different choices of $\triangle R$. In the calculation of preformation probability P_0, the mass- and charge-dispersion concepts are introduced through the mass- ($\eta_A = \frac{|A_1-A_2|}{A_1+A_2}$) and charge-asymmetry ($\eta_Z = \frac{|Z_1-Z_2|}{Z_1+Z_2}$) coordinates, which are treated as the dynamical factors in the collective clusterization approach of DCM. It is known that the decaying binary fragments with the minimum value of the fragmentation potential possess the highest preformation probability P_0. In other words, it can be said that, the term P_0 shows an inverse trend compared to that of $V(\eta)$ observed in Fig. 5. The fission fragments observed in the near-symmetric and asymmetric regions in both the mass- and charge-distribution cases are almost similar. On the basis of the above observation, we have calculated the fission cross sections (σ^{DCM}_{fis}) using DCM for both the mass and charge distributions of ^{224}Th*, formed from the ^{16}O + ^{208}Pb reaction,

TABLE I. The detail of calculated fission cross sections σ_{fis}^{DCM} (mb) of the $^{16}O + ^{208}Pb \rightarrow ^{224}Th^*$ reaction with the inclusion of deformation up to β_3 and related cold optimum orientation ($\theta_{\rm opt}^{\beta_2}$ and $\theta_{\rm opt}^{\beta_2,\beta_3}$). For comparison, the experimental data [34] of the above mentioned reaction are also given.

E_{CN}^*	$E_{\rm c.m.}$	T	$\sigma_{fis}^{\rm Expt.}$	ΔR (fm)		$\ell_{\max}$ ($\hbar$)		σ_{fis}^{DCM} (mb)	
(MeV)	(MeV)	(MeV)	(mb)	β_2	β_2, β_3	β_2	β_2, β_3	β_2	β_2, β_3
			$^{224}Th^* \longrightarrow A_1 + A_2$						
22.65	68.69	0.974	0.00844 ± 0.0035	0.80	0.81	92	104	0.00649	0.00845
23.46	69.49	0.991	0.04624 ± 0.0145	0.81	0.87	95	105	0.0438	0.0431
24.37	70.41	1.009	0.4869 ± 0.137	0.98	1.05	95	105	0.452	0.491
25.29	71.33	1.028	2.1503 ± 0.634	1.00	1.08	98	108	2.201	2.0464
			$^{224}Th^* \longrightarrow Z_1 + Z_2$						
22.65	68.69	0.974	0.00844 ± 0.0035	0.25	0.30	111	123	0.00545	0.00866
23.46	69.49	0.991	0.04624 ± 0.0145	0.28	0.35	116	125	0.0428	0.0361
24.37	70.41	1.009	0.4869 ± 0.137	0.42	0.48	118	126	0.305	0.335
25.29	71.33	1.028	2.1503 ± 0.634	0.55	0.56	120	132	1.504	2.595

at energies below the Coulomb barrier. The details of theoretically and experimentally obtained σ_{fis} for the above mentioned reaction are given in Table I. The calculations were done initially with the inclusion of β_2 deformation and related cold optimum orientation ($\theta_{\rm opt}^{\beta_2}$). Subsequently, the experimental data were addressed within the permissible values of ΔR, for incident beam energies $E_{\rm c.m.} = 68.69$–71.33 MeV. In the above calculations, the values of $\ell_{\max}$ are obtained at a point when there is no contribution of light particle. Later, due to involvement of deformations (up to β_3) along with $\theta_{\rm opt}^{\beta_2,\beta_3}$, there is an increment in $\ell_{\max}$ of about 10%, and the obtained σ_{fis}^{DCM} are found closer to $\sigma_{fis}^{\rm Expt.}$. However, there is a very small change in ΔR. Apart from this, one can also notice from Table I that the neck-length parameter decreases significantly, as one moves from the mass-distribution to the charge-distribution criteria. This means, for the charge-dispersion case, that the interaction among decaying fragments takes place at relatively smaller distance than in the mass dispersion/distribution of an excited compound nucleus.

Based on the above observations related to the neck-length parameter and $\ell_{\max}$ values, the fission dynamics of all considered isotopes of $^{222,224,226,228,230}Th^*$ has been studied using DCM. There is a very small difference in ΔR and $\ell_{\max}$ values, while studying the fission dynamics of isotopes of a compound nucleus [60,61]. Thus, for decay analysis of even-even isotopes of $^{222\text{–}230}Th^*$ via mass distribution at $E_{CN}^* = 24.37$ MeV, we have considered common values $\Delta R = 1.0$ fm and $\ell_{\max} = 100\hbar$, using the systematics of the ^{224}Th compound nucleus. Similarly, for charge distribution which takes place comparatively at smaller distance, $\Delta R = 0.45$ fm and $\ell_{\max} = 120\hbar$ values can be taken into account.

B. Mass and charge dispersions of even-even isotopes of $^{222\text{–}230}Th^*$

The study based on fusion-fission phenomena is not only for the calculation of fission cross section, but it also provides the idea of symmetric/asymmetric mass and charge fragments produced during the disintegration of an excited CN. In view

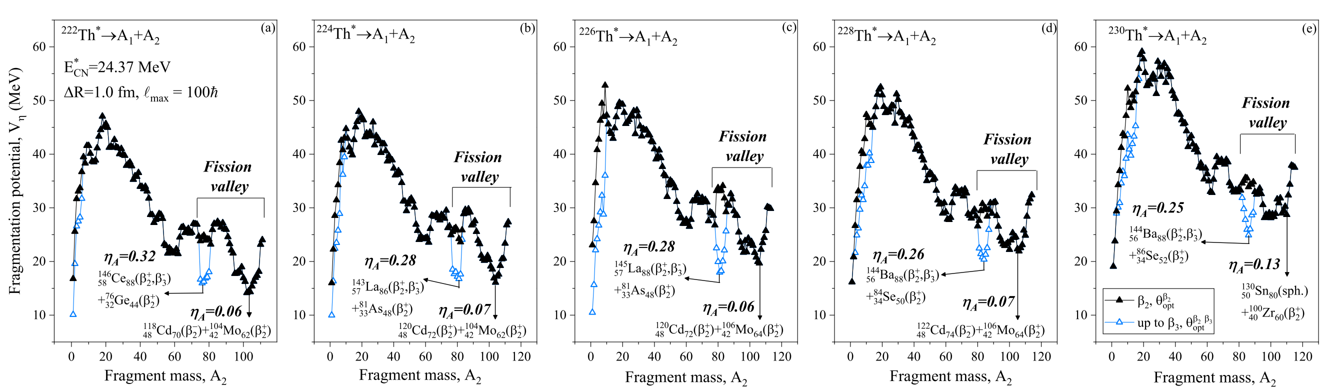

FIG. 6. The variation of fragmentation potential $V(\eta)$ is plotted as a function of mass number A_2, first with the inclusion of quadrupole β_2 deformation (and related cold optimum orientation $\theta_{\rm opt}^{\beta_2}$) and second with octupole β_3 deformation (and $\theta_{\rm opt}^{\beta_2\beta_3}$) of the decaying fragment, for the decay analysis of even-even isotopes of $^{222\text{–}230}Th^* \rightarrow A_1 + A_2$, at a common excitation energy $E_{CN}^* = 24.37$ MeV.

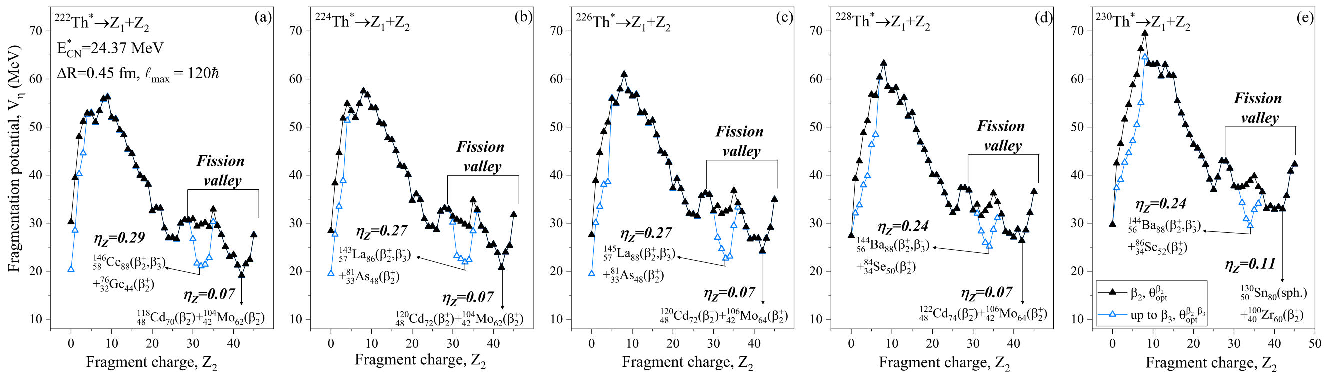

FIG. 7. Same as Fig. 6, but the variation of $V(\eta)$ is shown with respect to charge number Z_2 of even-even isotopes of $^{222–230}$Th$^* \rightarrow Z_1 + Z_2$.

of this, the structure of fragmentation potential $V(\eta)$ is shown in Fig. 6 with respect to the mass number A_2 of decaying fragments from ^{222,224,226,228,230}Th*. The region of interest that is the fission valley is marked in this figure. Interestingly, two minima are observed in the fragmentation potential for the considered isotopes of Th which belong to near-symmetric and asymmetric mass regions. The near mass-symmetric region corresponds to the quadrupole (β_2) deformed fragments of elongated configuration, whereas the presence of octupole deformation in one of the decaying nuclear partners minimizes the fragmentation potential in the mass-asymmetric region ($\eta_A \approx 0.3$). Moreover, one can notice in Fig. 6(a) for ^{222}Th* that the near-symmetric fission shows deeper minima in $V(\eta)$ as compared to the asymmetric fission fragments. For the ^{224}Th* case represented in Fig. 6(b), the minimum of $V(\eta)$ observed in the asymmetric fission starts competing with the near-symmetric dip. Moving ahead, a transition is observed for heavy-mass isotopes, i.e., ^{226,228,230}Th*, as shown in panels (c)–(e) of Fig. 6. In other words, the minimum in $V(\eta)$ becomes relatively deeper for octupole deformed fragments present in the asymmetric region, than that of near-symmetric quadrupole deformed fragments. Similar results have been observed while studying the "charge dispersion" of even-even isotopes of $^{222–230}$Th*, as shown in panels (a)–(e) of Fig. 7. Note that, in both the mass- and charge-dispersion cases, the fission fragments observed at deep valley locations are identical.

In Table II, we show the atomic and neutron numbers, respectively at the left and right subscripts, of near-symmetric and asymmetric fission fragments along with their quadrupole (β_{2i}) and octupole (β_{3i}) deformations and related cold optimum orientations ($\theta_{\rm opt}^{\beta_2}$ and $\theta_{\rm opt}^{\beta_2\beta_3}$). It is known that the minimization in fragmentation potential occurs due to shell stabilization, which generally occurs for a magic number of nucleons, either in one or both the fission fragments. On the basis of this fact, analysis shows that in the near-symmetric region the fission fragments are quadrupole deformed and one of them, in decaying from light mass isotopes of Th (^{222,224}Th*), has neutron number equal to 62, which is a deformed magic number and provides shell stabilization [22]. On the other hand, in the asymmetric fission region of heavy-mass isotopes (^{226,228,230}Th*), the decaying fragment of up to octupole deformation has atomic number close or equal to 56. In the recent experimental works [24,27,62], it has been shown that the nucleus of atomic number 56 (of element ^{156}Ba), or close to it, possessing octupole deformation, gives extra stability. Due to these facts, one can see minimization in $V(\eta)$ with prominent effect. In addition to the above, one can also notice from Table II that, in the near-symmetric region, the magnitude of β_{21} for fragment A_1 is decreasing and becomes zero, as one goes from ^{224}Th* to ^{230}Th* cases. On the other hand, in the asymmetric region, one of decay fragments is octupole deformed and another is quadrupole deformed.

TABLE II. The details of the most probable fission fragments of quadrupole (β_{2i}; here $i = 1, 2$) and octupole deformation (β_{3i}) along with their related cold optimum orientations ($\theta_{\rm opt}^{\beta_2}$ [7] and $\theta_{\rm opt}^{\beta_2\beta_3}$ [25]) found respectively in the near mass/charge-symmetric and -asymmetric fission regions of even-even isotopes of $^{222–230}$Th* compound nuclei.

	Near mass/charge-symmetric region					Mass/charge-asymmetric region						
CN*	Fission fragments	β_{21}	β_{22}	$\theta_{\rm opt}^{\beta_{21}}$	$\theta_{\rm opt}^{\beta_{22}}$	Fission fragments	β_{21}	β_{31}	β_{22}	β_{32}	$\theta_{\rm opt}^{\beta_{21}\beta_{31}}$	$\theta_{\rm opt}^{\beta_{22}\beta_{32}}$
^{222}Th*	$^{118}_{48}$Cd$_{70}$ + $^{104}_{42}$Mo$_{62}$	−0.238	0.377	90°	180°	$^{146}_{58}$Ce$_{88}$ + $^{76}_{32}$Ge$_{44}$	0.182	−0.116	0.143	0.0	0°	180°
^{224}Th*	$^{120}_{48}$Cd$_{72}$ + $^{104}_{42}$Mo$_{62}$	0.140	0.377	0°	180°	$^{143}_{57}$La$_{86}$ + $^{81}_{33}$As$_{48}$	0.154	−0.104	0.163	0.0	0°	180°
^{226}Th*	$^{120}_{48}$Cd$_{72}$ + $^{106}_{42}$Mo$_{64}$	0.140	0.377	0°	180°	$^{145}_{57}$La$_{88}$ + $^{81}_{33}$As$_{48}$	0.173	−0.128	0.163	0.0	0°	180°
^{228}Th*	$^{122}_{48}$Cd$_{74}$ + $^{106}_{42}$Mo$_{64}$	−0.104	0.354	90°	180°	$^{144}_{56}$Ba$_{88}$ + $^{84}_{34}$Se$_{50}$	0.164	−0.126	0.053	0.0	0°	180°
^{230}Th*	$^{130}_{50}$Sn$_{80}$ + $^{100}_{40}$Zr$_{60}$	0.00	0.364	0°	180°	$^{144}_{56}$Ba$_{88}$ + $^{86}_{34}$Se$_{52}$	0.164	−0.126	0.125	0.0	0°	180°

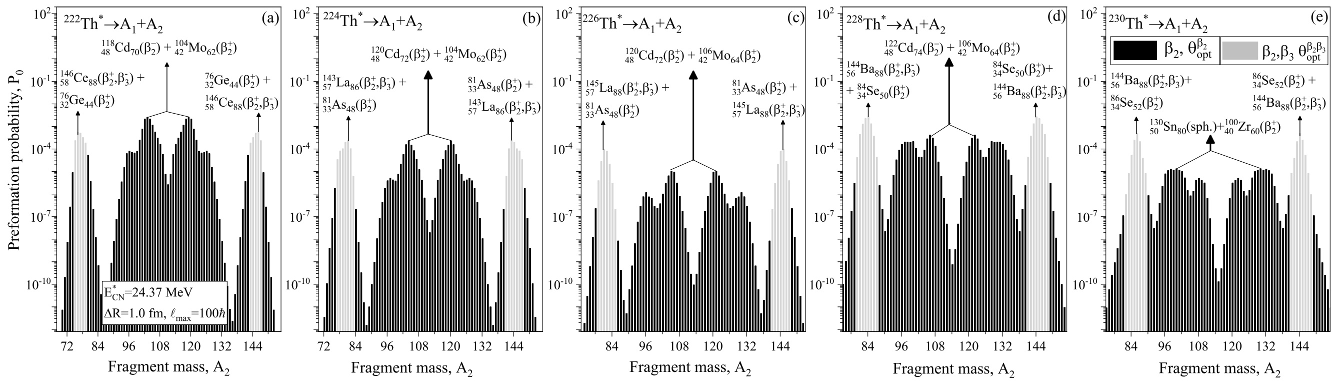

FIG. 8. The variation of preformation probability P_0 as a function of mass number of the decaying fragment (A_2) from the even-even isotopes of $^{222-230}Th^* \to A_1 + A_2$ is shown, first with the inclusion of quadrupole β_2 deformation and related optimum orientation ($\theta_{opt}^{\beta_2}$) and second with higher-order deformations (up to β_3) and $\theta_{opt}^{\beta_3}$ being involved.

Here, the magnitude of β_{31} is relatively larger for fragment A_1 of heavy-mass isotopes of Th ($^{226,228,230}Th^*$), as compared to that of light-mass isotopes. In our recent work [26] we said that, for larger magnitude of β_3, the elongated configuration of octupole deformed nuclei enlarges the interaction distance to a large extent and gives relatively lower barrier height. As a consequence, one can notice the corresponding effects in the fragmentation potential. From above analysis, one can notice that the presence of deformations as well as shell-stabilization (due to magicity in nucleon number) play a significant role in the fission valley of Th.

Further, the role of deformation and orientation effect has been explored in the calculation of preformation probability P_0 as a function of mass and charge number of fission fragments preformed inside the even-even isotopes of $^{222-230}Th^*$, at a common excitation energy $E^*_{CN} = 24.37$ MeV. It is known that the fragments for which the fragmentation potential gets minimized have the highest preformation probability. In a recent work [63], a transition of symmetric to asymmetric fission has been shown as one moves from ^{222}Th to ^{230}Th compound nuclei. Additionally, in Ref. [64], the charge distribution of $^{222,224}Th$ isotopes shows a rise in the asymmetric region, but lower than that in symmetric fission, for excitation energy more than 11 MeV. Our calculations are in agreement with these observations. To show this, the preformation probabilities (P_0) of even-even isotopes of $^{222-230}Th^*$ are discussed and also shown in Figs. 8 and 9 respectively for mass- and charge-dispersion cases. It is clear from these figures that the octupole deformed nuclei always appear in the asymmetric mass regions, irrespective of the choice of mass and excitation energy range considered in the present work. In the above analysis, the near-symmetric fission is found to be dominant over asymmetric fission for the $^{222}Th^*$ case, at $E^*_{CN} = 24.37$ MeV. For $^{224}Th^*$, the contribution of near-symmetric and asymmetric components is comparable. On the other hand, for heavy-mass isotopes $^{226,228,230}Th^*$, the octupole deformed decaying nuclear partner of atomic number equal or close to 56 (^{145}La and ^{144}Ba) in the asymmetric region shows dominant behavior. In other words, it can be said that the asymmetric fission fragments of octupole-quadrupole deformed kind ($^{145}La + {}^{81}As$, $^{144}Ba + {}^{84}Se$, and $^{144}Ba + {}^{86}Se$) enhance the preformation probability P_0 to a larger extent. Also, in a recent experimental work [27], the authors gave evidence of pear-shape nuclei (i.e., ^{144}Ba) in the asymmetric region of heavy-mass actinides, and the present work is in line with the result of this paper.

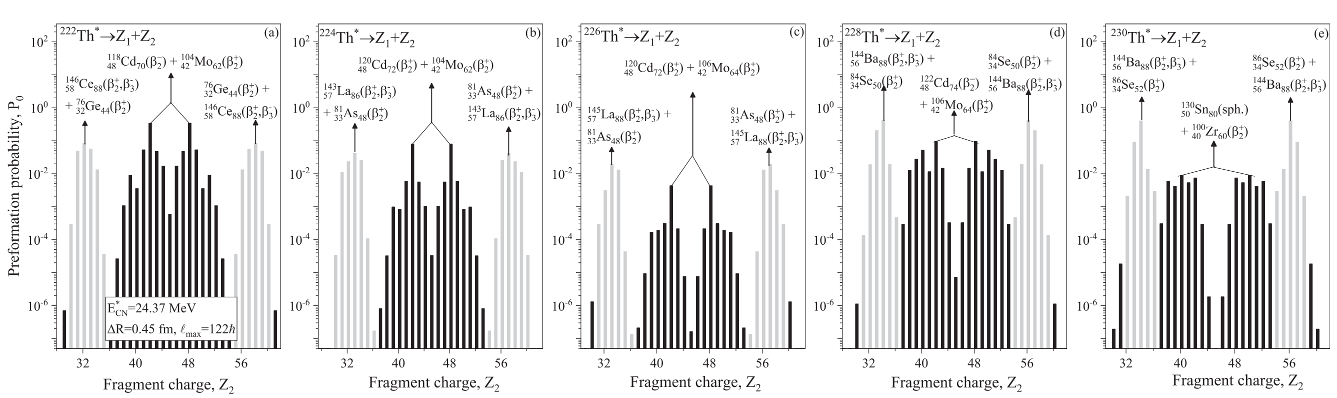

FIG. 9. Same as Fig. 8, but for the charge dispersion case, i.e., $^{222-230}Th^* \to Z_1 + Z_2$.

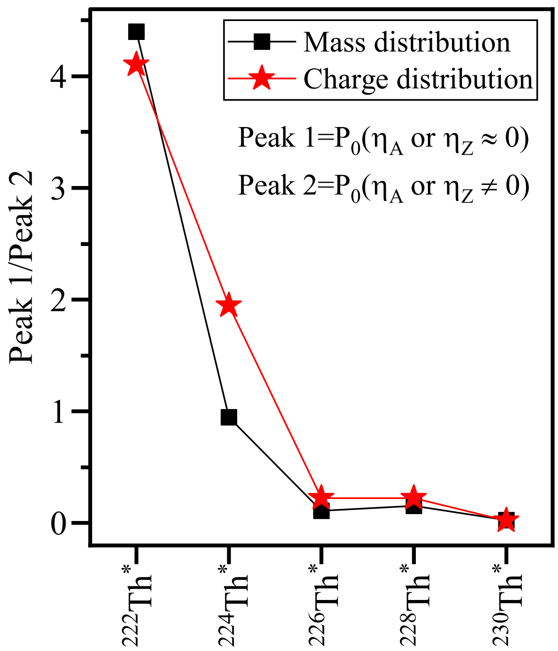

FIG. 10. The ratio of Peak 1 [$=P_0(\eta_A$ or $\eta_Z \approx 0)$] and Peak 2 [$=P_0(\eta_A$ or $\eta_Z \neq 0)$] obtained for even-even isotopes of ^{A}Th*, here $A = 222$, 224, 226, 228, and 230, at a common excitation energy, $E^*_{CN} = 24.37$ MeV.

Further, the ratio of the preformation probability P_0 peak obtained near the symmetric region (Peak 1) and the one in the asymmetric region (Peak 2) is shown in Fig. 10 for ^{222,224,226,228,230}Th* fission nuclei. In this figure, the ratio $(\frac{\text{Peak 1}}{\text{Peak 2}})$ is obtained for both the mass- and charge distributions of the above mentioned compound nuclei. It is observed that, the peak ratio decreases with increase in mass number of compound nuclei. Clearly, the lighter-mass compound nuclei prefer near-symmetric fragmentation of quadrupole-quadrupole deformed pairs of fission fragments. However, asymmetric fission of octupole-quadrupole deformed fragments is prominent in the heavier isotopes, i.e., ^{226,228,230}Th*.

IV. SUMMARY

In this paper, we have included the deformations up to β_3 and related cold optimum orientation (θ_{opt}), within the dynamical cluster-decay model, to study the nuclear fission dynamics of even-even isotopes of thorium, i.e., $^{222-230}$Th*. The above analysis was carried out at low excitation energy, which corresponds to the cold optimum configurations of the nuclei involved.

Initially, the neck-length parameter $\triangle R$ was optimized in reference to the available experimental data of fission cross sections of ^{224}Th*, formed via ^{208}Pb-based reaction, at below-barrier energies. Subsequently, the dips of fragmentation potential and corresponding peaks of preformation probability were analyzed in the near-symmetric (η_A and $\eta_Z \approx 0$) and asymmetric fission (η_A and $\eta_Z \neq 0$) regions of considered isotopes. It is observed that octupole deformed fragments appear in the asymmetric region, irrespective of the mass of Th isotopes. Note that, for both the mass- as well as charge-dispersion fragmentations, the most probable fission fragments observed are found to be identical. In the decay of light-mass isotopes of Th, i.e., ^{222,224}Th*, the near-symmetric fission is preferred due to deformed magic number of neutrons ($N = 62$) of the quadrupole deformed fragment. However, the asymmetric fission involving an octupole deformed fragment ($Z = 56$; ^{144}Ba or in its vicinity) is found to be prominent in the case of heavier isotopes of Th, i.e., ^{226,228,230}Th*. From above analysis, the near-symmetric and asymmetric fission modes observed in the decay of Th isotopes, due to involvement of deformations (up to β_3) and related cold optimum orientation, are in agreement with the experimental results.

Such investigations help in understanding sfission dynamics, especially in the asymmetric region of heavy-mass actinides. For further studies, one can explore the relevance and importance of octupole deformed fragments decaying from heavy and superheavy nuclei.

ACKNOWLEDGMENTS

Financial support of Senior Research Fellowship (SRF) from Council of Scientific & Industrial Research (CSIR), File No. 09/0667(11160)/2021-EMR-I; a research project of Department of Atomic Energy (DAE), Government of India, Sanction No. 58/14/12/2019-BRNS and UGC-DAE consortium for Scientific Research, File No. UGC-DAE-CSR-KC/CRS/19/NP09/0920, are gratefully acknowledged. We also would like to show our gratitude to Dr. Dalip Verma, Central University of Himachal Pradesh and Late Prof. Raj K. Gupta, Panjab University for their suggestions on collective clusterization approach.

[1] S. Hoafmann and G. Munzenberg, Rev. Mod. Phys. **72**, 733 (2000).
[2] S. Hofmann *et al.*, Eur. Phys. J. A **14**, 147 (2002).
[3] Y. T. Oganessian, V. K. Utyonkov, Y. V. Lobanov, F. S. Abdullin, A. N. Polyakov, I. V. Shirokovsky, Y. S. Tsyganov, G. G. Gulbekian, S. L. Bogomolov, B. N. Gikal, A. N. Mezentsev, S. Iliev, V. G. Subbotin, A. M. Sukhov, A. A. Voinov, G. V. Buklanov, K. Subotic, V. I. Zagrebaev, M. G. Itkis *et al.*, Phys. Rev. C **70**, 064609 (2004).
[4] Y. T. Oganessian, J. Phys. G **34**, R165 (2007).
[5] U. Brosa, S. Grossmann, and A. Muller, Phys. Rep. **197**, 167 (1990).
[6] K. Nishio, H. Ikezoe, S. Mitsuoka, I. Nishinaka, Y. Nagame, Y. Watanabe, T. Ohtsuki, K. Hirose, and S. Hofmann, Phys. Rev. C **77**, 064607 (2008).
[7] R. K. Gupta *et al.*, J. Phys. G: Nucl. Part. Phys. **31**, 631 (2005).
[8] A. Sandulescu *et al.*, Phys. Lett. B **60**, 225 (1976).
[9] R. K. Gupta, A. Sandulescu, and W. Greiner, Phys. Lett. B **67**, 257 (1977).

[10] R. K. Gupta, C. Parvulescu, A. Sandulescu, and W. Greiner, Z. Phys. A **283**, 217 (1977).
[11] R. K. Gupta, A. Sandulescu, and W. Greiner, Z. Natureforsch. **32**, 704 (1977).
[12] A. Sandulescu, D. N. Poenaru, and W. Greiner, Fiz. Elem. Chartiz At. Yadra **11**, 1334 (1980) [Sov. J. Part. Nucl. **11**, 528 (1980)].
[13] D. N. Poenaru *et al.*, J. Phys. G: Nucl. Phys. **10**, L183 (1984).
[14] D. N. Poenaru, W. Greiner, M. Ivascu, and A. Sandulescu, Phys. Rev. C **32**, 2198 (1985).
[15] D. N. Poenaru and W. Greiner, J. Phys. G: Nucl. Part. Phys. **17**, S443 (1991).
[16] K.-H. Schmidt *et al.*, Nucl. Phys. A **665**, 221 (2000).
[17] D. N. Poenaru, Y. Nagame, R. A. Gherghescu, and W. Greiner, Phys. Rev. C **65**, 054308 (2002).
[18] D. N. Poenaru, R. A. Gherghescu, and W. Greiner, Phys. Rev. C **83**, 014601 (2011).
[19] M. Kaur, M. K. Sharma, and R. K. Gupta, Phys. Rev. C **86**, 064610 (2012).
[20] K.-H. Schmidt and B. Jurado, Rep. Prog. Phys. **81**, 106301 (2018).
[21] A. N. Andreyev, K. Nishio, and K.-H. Schmidt, Rep. Prog. Phys. **81**, 016301 (2018).
[22] A. Kaur, N. Sharma, and M. K. Sharma, Phys. Rev. C **103**, 034618 (2021).
[23] L. P. Gaffney *et al.*, Nature (London) **497**, 199 (2013).
[24] B. Bucher, S. Zhu, C. Y. Wu, R. V. F. Janssens, D. Cline, A. B. Hayes, M. Albers, A. D. Ayangeakaa, P. A. Butler, C. M. Campbell, M. P. Carpenter, C. J. Chiara, J. A. Clark, H. L. Crawford, M. Cromaz, H. M. David, C. Dickerson, E. T. Gregor *et al.*, Phys. Rev. Lett. **116**, 112503 (2016).
[25] S. Jain, M. K. Sharma, and R. Kumar, Phys. Rev. C **101**, 051601(R) (2020).
[26] S. Jain, M. K. Sharma, and R. Kumar, Chin. Phys. C **46** 014102 (2022).
[27] G. Scamps and C. Simenel, Nature (London) **564**, 382 (2018).
[28] R. K. Gupta, in *Clusters in Nuclei*, edited by C. Beck, Lectures Notes in Physics 818, Vol. I (Springer-Verlag, Berlin, 2010), p. 223.
[29] D. Jain, R. Kumar, and M. K. Sharma, Phys. Rev. C **87**, 044612 (2013).
[30] A. Kaur and M. K. Sharma, Phys. Rev. C **99**, 044611 (2019).
[31] H. J. Fink, J. Maruhn, W. Scheid, and W. Greiner, Z. Phys. **268**, 321 (1974).
[32] J. Maruhn and W. Greiner, Phys. Rev. Lett. **32**, 548 (1974).
[33] R. K. Gupta, W. Scheid, and W. Greiner, Phys. Rev. Lett. **35**, 353 (1975).
[34] M. Dasgupta, D. J. Hinde, A. Diaz-Torres, B. Bouriquet, C. I. Low, G. J. Milburn, and J. O. Newton, Phys. Rev. Lett. **99**, 192701 (2007).
[35] R. K. Gupta and W. Greiner, in *Heavy Elements and Related New Phenomena*, edited by W. Greiner and R. K. Gupta (World Scientific, Singapore, 1999), Vol. I, p. 536.
[36] R. K. Gupta, W. Scheid, and W. Greiner, Phys. Rev. Lett. **35**, 6 (1975).
[37] H. Kroger and W. Scheid, J. Phys. G **6**, L85 (1980).
[38] H. S. Khosla and S. S. Malik, Nucl. Phys. A **513**, 115 (1990).
[39] S. Kumar and R. K. Gupta, Phys. Rev. C **55**, 218 (1997).
[40] R. K. Gupta, S. Kumar, and W. Scheid, Int. J. Mod. Phys. E **06**, 259 (1997).
[41] S. J. Sanders, D. G. Kovar, B. B. Back, C. Beck, D. J. Henderson, R. V. F. Janssens, T. F. Wang, and B. D. Wilkins, Phys. Rev. C **40**, 2091 (1989).
[42] S. J. Sanders, Phys. Rev. C **44**, 2676 (1991).
[43] T. Matsuse, C. Beck, R. Nouicer, and D. Mahboub, Phys. Rev. C **55**, 1380 (1997).
[44] R. Dutt, A. Khare, and U. P. Sukhatme, Am. J. Phys. **59**, 723 (1991).
[45] N. J. Davidson *et al.*, Nucl. Phys. A **570**, 61 (1994).
[46] P. A. Seeger, Nucl. Phys. **25**, 1 (1961).
[47] S. DeBenedetti, *Nuclear Interactions* (Wiley & Sons, New York, 1964).
[48] W. Myers and W. J. Swiatecki, Nucl. Phys. **81**, 1 (1966).
[49] C. Y. Wong, Phys. Rev. Lett. **31**, 766 (1973).
[50] P. Möller, J. R. Nix, W. D. Myers, and W. J. Swiatecki, At. Data Nucl. Data Tables **59**, 185 (1995).
[51] A. Bohr, Mat. Fys. Medd. Dan. Vid. Selsk **26** (1952).
[52] A. Bohr and B. R. Mottelson, Mat. Fys. Medd. Dan. Vid. Selsk **27**, 16 (1953).
[53] S. Shlomo and J. B. Natowitz, Phys. Rev. C **44**, 2878 (1991).
[54] J. Blocki *et al.*, Ann. Phys. (NY) **105**, 427 (1977).
[55] K. J. LeCouteur and D. W. Lang, Nucl. Phys. **13**, 32 (1959).
[56] M. Seiwert, W. Greiner, V. Oberacker, and M. J. Rhoades-Brown, Phys. Rev. C **29**, 477 (1984).
[57] N. Malhotra and R. K. Gupta, Phys. Rev. C **31**, 1179 (1985).
[58] R. K. Gupta, N. Singh, and M. Manhas, Phys. Rev. C **70**, 034608 (2004).
[59] M. Manhas and R. K. Gupta, Phys. Rev. C **72**, 024606 (2005).
[60] M. K. Sharma, G. Sawhney, R. K. Gupta, and W. Greiner, J. Phys. G: Nucl. Part. Phys. **38**, 105101 (2011).
[61] N. Gover, I. Sharma, G. Kaur, and M. K. Sharma, Nucl. Phys. A **959**, 10 (2017).
[62] B. Bucher, S. Zhu, C. Y. Wu, R. V.F. Janssens, R. N. Bernard, L. M. Robledo, T. R. Rodriguez, D. Cline, A. B. Hayes, A. D. Ayangeakaa, M. Q. Buckner, C. M. Campbell, M. P. Carpenter, J. A. Clark, H. L. Crawford, H. M. David, C. Dickerson, J. Harker, C. R. Hoffman *et al.*, Phys. Rev. Lett. **118**, 152504 (2017).
[63] A. Chatillon, J. Taieb, H. Alvarez-Pol, L. Audouin, Y. Ayyad, G. Belier, J. Benlliure, G. Boutoux, M. Caamano, E. Casarejos, D. Cortina-Gil, A. Ebran, F. Farget, B. Fernandez-Dominguez, T. Gorbinet, L. Grente, A. Heinz, H. T. Johansson, B. Jurado, A. Kelic-Heil *et al.*, Phys. Rev. C **99**, 054628 (2019).
[64] H. Pasca, A. V. Andreev, G. G. Adamian, and N. V. Antonenko, Phys. Rev. C **94**, 064614 (2016).